JOURNAL OF SOLID STATE CHEMISTRY 118, 402–411 (1995)

Structural and Magnetic Properties of Transition Metal Arsenates, AAs_2O_6, A = Mn, Co, and Ni

A. M. Nakua and J. E. Greedan[1]

Institute for Materials Research, McMaster University, 1280 Main Street West, Hamilton, Ontario L8S 4M1, Canada

Received October 14, 1994; in revised form February 6, 1995; accepted February 7, 1995

The divalent transition metal arsenates with the general formula AAs_2O_6, where A is Mn, Co, Ni, were prepared. Their crystal structures were refined using the Rietveld profile method with neutron powder diffraction data in the space group P-31m. $NiAs_2O_6$ has the unit cell dimensions (Å) a = 4.7585(7), c = 4.4349(4), Z = 1, and V = 86.97 Å^3; for $CoAs_2O_6$, a = 4.7768(12), c = 4.4968(8), and V = 88.09 Å^3; and for $MnAs_2O_6$ a = 4.7956(9), c = 4.6923(6), and V = 93.45 Å^3. Magnetic properties were examined down to 5 K. Magnetic susceptibility data reveal the presence of long-range order in these materials, while higher temperature data resemble those of a simple antiferromagnet and no indication of the presence of any short-range order was observed except in the case of $NiAs_2O_6$, in which rather weak ferromagnetic correlations were detected. The magnetically ordered state was investigated by the use of the low-temperature neutron diffraction. $NiAs_2O_6$ and $CoAs_2O_6$ have the same propagation vector, k = (00½), while an incommensurate magnetic structure was observed for $MnAs_2O_6$, in which the magnetic superlattice reflections were indexed with the propagation vector k = (0.055, 0.389, 0.136). These results are compared with the phase diagrams of Reimers and Dahn for a triangular lattice with ..AAA.. stacking. © 1995 Academic Press, Inc.

INTRODUCTION

For a number of years, the complex oxides of the general formula AB_2O_6, where A is a divalent transition metal ion and B is a pentavalent diamagnetic cation such as Sb^{5+}, Ta^{5+}, or As^{5+}, have been extensively studied in our laboratory (1–3). Of particular interest have been their crystal structures and magnetic properties and the correlations between them. These oxides are found to crystallize mainly in two structure types. The trirutile structure is found for most of the transition metal tantalates and transition metal antimonates, except for $MnSb_2O_6$ and $CuTa_2O_6$. The second structure type is the lead antimonate, $PbSb_2O_6$, structure, which is adopted by the transition metal arsenates, AAs_2O_6, in which the cations A^{2+} and B^{5+} are segregated into different layers. These two structure types are highly ordered due to the large difference in the formal charges of the cations A and B.

Transition metal antimonates and tantalates were studied extensively in the past few years and were reviewed by Greedan recently (3). As for the transition metal arsenates, little has been published since they were reported by Magneli in 1941 (4), who synthesized and determined the cell parameters of cobalt arsenate along with some alkali earth arsenates. Taylor and Hyde (5) then reported the synthesis and cell parameters of $CoAs_2O_6$ and $NiAs_2O_6$, which were in accordance with those reported previously by Magneli. Later, Kasper (6) investigated the spectrophotometrical properties of $CoAs_2O_6$ and $NiAs_2O_6$ among other oxides of the general formula AB_2O_6.

Detailed studies of the crystal structures or the magnetic properties of these compounds had not been reported. With respect to their crystal structures, Magneli had proposed that these arsenates adopted the lead antimonate, $PbSb_2O_6$, structure with the A^{2+} and As^{5+} atoms assigned to special positions in the space group $P312$, and the oxygen atom coordinates were determined from crystal–chemical considerations. Subsequently, Hill (7) has examined the $PbSb_2O_6$ structure and has concluded that the correct space group is P-31m. It is of interest here to determine which space group is appropriate for the AAs_2O_6 phases.

In this paper the crystal structure and magnetic properties of the transition metal arsenates AAs_2O_6, where A is Ni, Co, Mn, are reported. The preparation of $MnAs_2O_6$ was attempted for the first time. Often compounds of Co^{2+} (r = 0.745 Å) and Ni^{2+} (r = 0.690 Å) are isostructural (8) while the larger Mn^{2+} (r = 0.830 Å) sometimes adopts a different structure type as in the case of the transition metal antimonates. The stability range of the $PbSb_2O_6$ structure is dependent on the ratio of the ionic radii of A and B ions. As far as the arsenates are concerned, the upper and lower limits for the radius ratio (A^{2+} : As^{5+}) are 2.6 and 1.5 according to Hill (7), which

[1] To whom correspondence should be addressed.

0022-4596/95 $12.00

suggests that $MnAs_2O_6$ should also adopt the $PbSb_2O_6$ structure.

The transition metal sublattice in these materials forms layers of hexagonal nets stacked in an ...AAA... fashion. Reimers and Dahn (9) have recently studied the magnetic phase diagrams of this and other stacking sequences for hexagonal lattices in the mean field approximation and it is of interest to compare the observed magnetic properties with these predictions.

EXPERIMENTAL

1. *Sample preparation.* These arsenates were prepared by a solid state reaction of a 1 : 1 molar ratio of arsenic pentoxide and the transition metal oxides, *M*O. Due to the high hygroscopicity of the arsenic pentoxide, careful drying procedures had to be followed. The moisture content of the pentoxide was determined by the use of thermogravimetric analysis, TGA, for every preparation, which typically was found to be in the range 14–20 wt%.

A careful drying procedure was necessary for these preparations to be successful. All the weighing and mixing were done in a dry box, and the mixture was pressed into pellets and transferred as quickly as possible to a quartz tube which then was dried under vacuum as follows: the mixture of *M*O and As_2O_5 was heated at 100°C for 24 hr and at 200°C for 30 to 40 hr depending on the moisture content. The dehydration of the pentoxide can be represented by the following chemical reaction (10):

$$As_2O_5 \cdot xH_2O \rightarrow H_5As_3O_{10} \rightarrow As_2O_5.$$

The tube is then sealed under 1×10^{-5} Torr and soaked for one week at 650–750°C. The quartz tubes were protected by a ceramic tube during the firing. In the course of these preparations, severe attack of the quartz tubes was observed.

NiO (AESAR, 99.998%) and As_2O_5 (AESAR, 99.99%) were heated to 700°C for one week. The yellow color of the product was consistent with that reported by Taylor and Hyde (5). It was verified by the use of the powder X-ray diffraction that the product was single phase. The reaction of CoO (ALFA Inorganics) and As_2O_5 (AESAR, 99.99%) yielded a purple product which was analyzed to be a single phase and of the composition $CoAs_2O_6$. This reaction mixture was heated at 650°C for four days.

Identical procedures were used in the case of the manganese arsenate where a mixture of MnO (AESAR, 99.5%) and As_2O_5 (AESAR, 99.99%) was heated to 700°C for one week. A pinkish white product was obtained which has an X-ray powder pattern very similar to that of the cobalt and nickel counterparts. The cell parameters were determined by least-squares fit of the scanned data from the Guinier film.

2. *X-Ray Diffraction*

The cell parameters were determined by the use of a Guinier–Hagg camera (IRDAB XDC700) with Cu$K\alpha$1 radiation and a Si standard. The Guinier films were read with a computer-controlled, automated LS-20 type line scanner (KEJ Instruments, Töby, Sweden). Using the output of the scanner, the cell parameters were refined using the LSUDF least-squares program. These cell parameters were then used in the Rietveld refinement fittings.

3. *Neutron Diffraction*

Room-temperature and low-temperature neutron data were collected at the McMaster Nuclear Reactor, MNR, with 1.39-Å neutrons. The detector was a three-tube position sensitive detector which has been described previously (11). The sample holder for the room-temperature experiments was a thin-walled vanadium can while that for the low-temperature experiments was an aluminum can with helium exchange gas which ws sealed with an indium gasket. Low-temperature neutron diffraction data for $MnAs_2O_6$ were collected at the Dualspec diffractometer at Chalk River labs with 1.45-Å neutrons.

Nuclear structure refinements were carried out by the Rietveld profile method using DBWS9006PC by Sakthivel and Young (12). Magnetic structures were refined using the RIETAN program written by Izumi (13) which is capable of modeling neutron scattering from magnetic structures with collinear spin arrangements. The magnetic moment of each magnetic site and the angle between the spin direction and the unique axis of the unit cell can be refined using the equations given by Shirane (14). Magnetic form factors were taken from Watson and Freeman (15).

4. *Magnetic Susceptibility*

Magnetic susceptibility data were collected with a Quantum Design SQUID magnetometer using a pressed polycrystalline pellet. The magnetometer was calibrated with a high-purity palladium sample.

RESULTS AND DISCUSSION

Crystal Structures

In the course of the refinement of these arsenates, the structure was described, initially, in the space group *P*312, i.e., the Magneli model, with the A^{2+} ion fixed at

TABLE 1
Refinement Conditions for AAs_2O_6 Compounds

	$NiAs_2O_6$	$CoAs_2O_6$	$MnAs_2O_6$
a(Å)	4.4785(7)	4.7768(12)	4.7956(9)
c(Å)	4.4349(4)	4.4968(8)	4.6923(6)
Volume(Å^3)	86.97	88.09	93.45
Space group	P-31m	P-31m	P-31m
2θ range	10-115	12-113	12-100
No. data points	1070	1030	980
Independent reflections	93	86	100
No. parameters refined	18	18	18
$*R_{wp}$[a]	7.85%	8.51%	8.13%
R_p	6.07%	6.59%	5.98%
R_I	6.82%	7.11%	4.39%
R_{exp}	2.5%	2.59%	3.10%

[a] $R_{wp} = 100[\Sigma\, w_i(Y_{obs} - Y_{cal})^2/\Sigma\, w_i\, Y_{obs}]^{\frac{1}{2}}$; $R_p = 100\ (\Sigma|Y_{obs} - Y_{cal}|/\Sigma|Y_{obs}|)$; $R_I = 100\ [(\Sigma|I_{obs} - I_{cal}|)/\Sigma\, I_{obs}]$; $R_{exp} = 100\ [(N - P + C)/\Sigma\, w_i Y_{obs}]^{\frac{1}{2}}$.

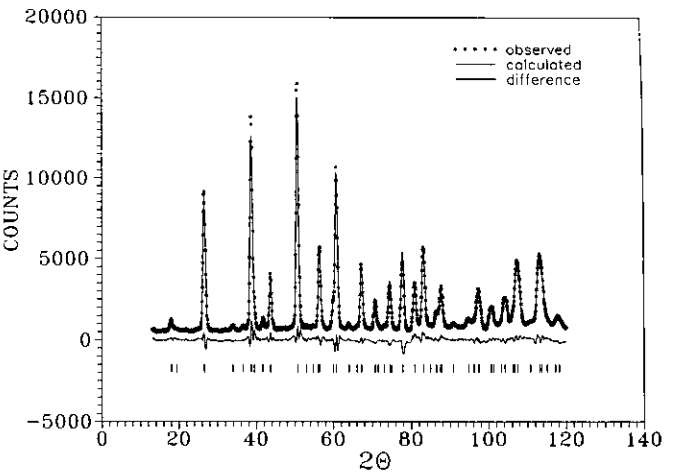

FIG. 1. The Rietveld refinement pattern of neutron diffraction data for $NiAs_2O_6$. The asterisks represent the observed profile, the solid line is the calculated profile, the difference is plotted below, and the vertical bars indicate the Bragg peak positions.

the origin, the As^{5+} ion distributed over two special positions, 1d ($\frac{1}{3}$, $\frac{2}{3}$, $\frac{1}{2}$) and 1f ($\frac{2}{3}$, $\frac{1}{3}$, $\frac{1}{2}$), and the O atoms assigned to the general position 6l with the coordinates (x, 0, z). The refinement results confirmed the general atomic arrangements proposed by Magneli, but some problems were noticed such as the instability of the refinement, the negative temperature factors, and the lack of convergence when the O atom coordinates were released. These problems were similar to those encountered by Hill (7) in the refinement of the crystal structure of $PbSb_2O_6$ which was subsequently refined in the space group P-31m. The results found here confirm the prediction of Hill that the space group P312 has an unnecessarily low symmetry for the AB_2O_6 arsenates.

Thus, a full-matrix least-squares refinement in P-31m with 18 variable parameters was performed on the neutron diffraction data for each of the three phases. The refined variables included a scale factor, cell parameters, positional parameters, isotropic thermal parameters, asymmetry, preferred orientation, and background and profile parameters. Data collection conditions and refinement details of all three phases are summarized in Table 1. Atomic parameters are listed in Table 2 while selected bond distances and bond angles are tabulated in Table 3.

For $NiAs_2O_6$, the Rietveld refinement fit is plotted in Fig. 1. The NiO_6 octahedron is very symmetric with a Ni–O bond distance of 2.098(6) Å, which is in accordance with the sum of the ionic radii of both ions (2.06 Å). Ni^{2+} appears to be situated in the center of the octahedron as indicated by the O–Ni–O bond angles. The As–O bond length is 1.827(2) Å, which is close to the sum of the ionic radii of As^{5+} and O^{2-} (1.86 Å).

In the case of $CoAs_2O_6$, similar results were obtained. Figure 2 plots the Rietveld refinement fit. The Co–O

TABLE 2
Atomic Positions for AAs_2O_6 Compounds

	Atom	Site	x	y	z	B (Å^2)
$NiAs_2O_6$	Ni	1a	0.0	0.0	0.0	0.16(6)
	As	2d	1/3	2/3	1/2	0.62(7)
	O	6k	0.3595(6)	0.0	0.2739(5)	0.49(4)
$CoAs_2O_6$	Co	1a	0.0	0.0	0.0	0.48(10)
	As	2d	1/3	2/3	1/2	0.30(7)
	O	6k	0.3626(6)	0.0	0.2759(7)	0.53(8)
$MnAs_2O_6$	Mn	1a	0.0	0.0	0.0	0.29(11)
	As	2d	1/3	2/3	1/2	0.81(6)
	O	6k	0.3704(3)	0.0	0.2835(5)	1.20(4)

TABLE 3
Selected Bond Distances and Bond Angles for AAs_2O_6

	$NiAs_2O_6$	$CoAs_2O_6$	$MnAs_2O_6$
A–O	2.098(4)	2.131(4)	2.214(4)
As–O	1.827(4)	1.830(3)	1.826(2)
O_c–A–O_c	180.0	180.0	180.0
O_c–A–O_c	89.84(5)	89.50(6)	89.84(5)
O_c–A–O_d	90.16(5)	90.50(6)	90.16(5)
O_a–As–O_f	82.52(6)	82.18(8)	81.39(6)
O_a–As–O_a	92.77(11)	92.58(10)	92.07(5)
O_a–As–O_c	173.23(12)	173.41(12)	170.33(6)

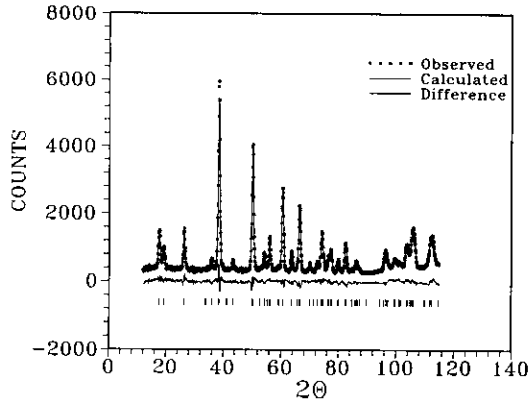

FIG. 2. The Rietveld refinement pattern of neutron diffraction data for $CoAs_2O_6$. The asterisks represent the observed profile, the solid line is the calculated profile, the difference is plotted below, and the bars indicate the Bragg peak positions.

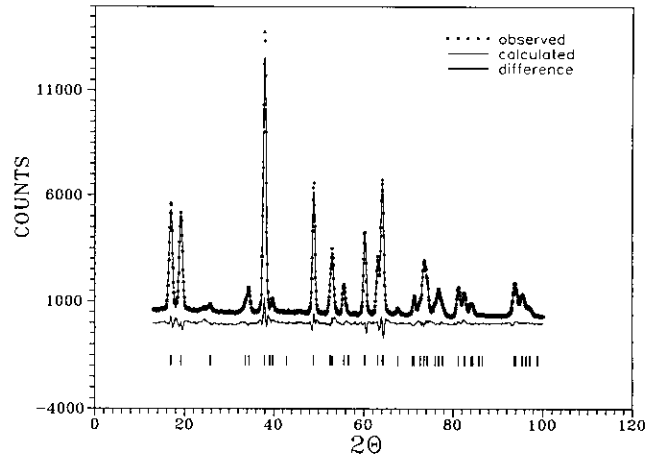

FIG. 3. The Rietveld refinement pattern of neutron diffraction data for $MnAs_2O_6$. The circles represent the observed profile, the solid line is the calculated profile, the difference is plotted below, and the bars indicate the Bragg peak positions.

bond length is 2.131(2) Å, which falls within the range of the reported values for the Co–O bond lengths (1.959–2.517 Å) (8). The As–O bond length of 1.830(3) Å is very similar to that for the $NiAs_2O_6$ compound. In a thorough study of the CoO_6 polyhedra in inorganic compounds, Wildner (8) surprisingly found that Co^{2+} ions generally reside in low-symmetry sites and that only 2% of the 112 $Co^{2+}O_6$ octahedra that were included in the study have the point symmetry $-3m$.

Regarding $MnAs_2O_6$, the Rietveld refinement fit is plotted in Fig. 3. The Mn–O bond distance obtained from the refinement is 2.214(3) Å, which compares well with the sum of the ionic radii with Mn^{2+} having a high spin electronic configuration (2.18 Å).

The framework of this structure type is based on a hexagonal close packed network of oxygen atoms filled with alternate layers of octahedral sites that are $\frac{2}{3}$ filled by As^{5+} ions and $\frac{1}{3}$ by the A^{2+} ions. This leads to sheets of edge-sharing AsO_6 octahedra, while the transition metal ions are located in isolated octahedral sites. This can be best seen in the (001) projection, Fig. 4. This structure is then best described as consisting of arsenic sheets formed by edge-sharing AsO_6 octahedra, whereas the transition metal ions are located in isolated octahedral sites with symmetry $-3m$ positioned above and below the vacant site, i.e., the centers of the rings in the arsenic layers, leading to a hexagonal magnetic sublattice with an ...AAA... stacking.

Magnetic Properties

I. Magnetic Susceptibility

Magnetic susceptibility data were measured on polycrystalline samples of each of the three compounds. Similar behavior was observed in all three phases. In a sharp contrast to the transition metal antimonates with the trirutile structure, there was no indication of the presence of any antiferromagnetic short-range order. This was apparent from the Curie–Weiss fits in which there were no deviations at lower temperatures except for $NiAs_2O_6$, as will be discussed, from the predictions of the Curie–Weiss law. In general, the magnetic susceptibilities of these compounds resemble those of a simple antiferromagnet. All three compounds exhibited what appears to be a magnetic long-range order transition at low temperatures.

Analysis of the magnetic susceptibility is outlined below. Magnetic long-range order in these compounds was investigated further with low-temperature neutron dif-

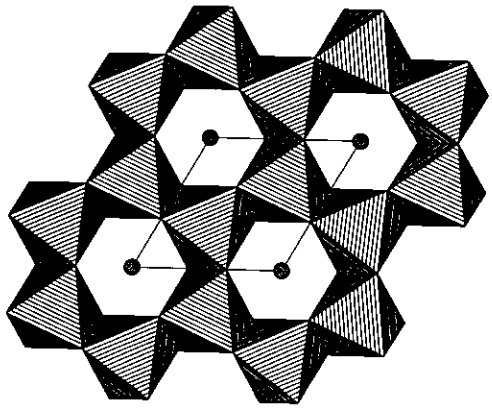

FIG. 4. (001) projection of the AAs_2O_6 structure. Polyhedra represent AsO_6 octahedra and the transition metal cations are represented as circles.

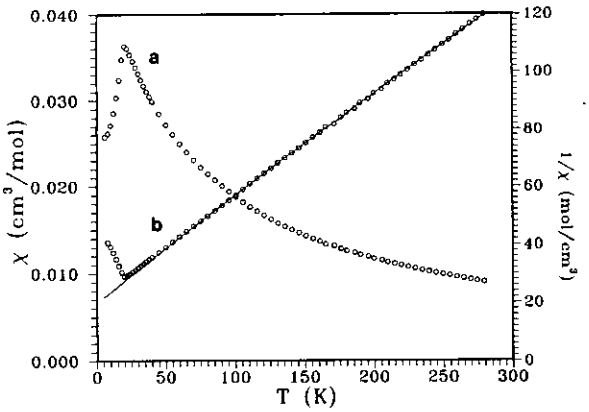

FIG. 5. (a) Magnetic susceptibility of the $CoAs_2O_6$; (b) the inverse of the magnetic susceptibility versus temperature. Circles represent the observed data and the solid line denotes the prediction of the Curie–Weiss fit.

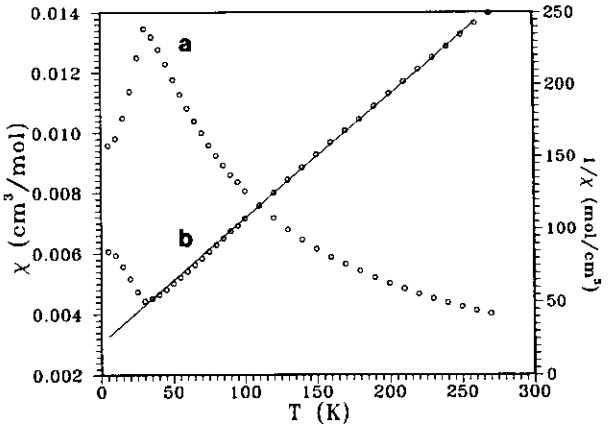

FIG. 6. (a) Magnetic susceptibility versus temperature for $NiAs_2O_6$; (b) the inverse of the magnetic susceptibility versus temperature. Circles represent the observed data and the solid line denotes the prediction of the Curie–Weiss fit.

fraction, a discussion of which will be delayed until the next section.

1. $CoAs_2O_6$. Figure 5 shows the magnetic susceptibility data as a function of temperature of $CoAs_2O_6$ at an applied field of 0.1 Tesla. The susceptibility attains a maximum of 3.63×10^{-2} emu/mole at $T = 20$ K and then drops sharply at lower temperatures. The data above the ordering temperature, between 50–270 K, were fitted to a Curie–Weiss law after correcting for core diamagnetism. The inverse susceptibility is plotted in Fig. 5. The fit gives an effective moment of 4.98(1) μ_B and a Weiss constant, θ, of −64.4(4) K. The effective magnetic moment of Co^{2+} in this compound falls within the acceptable range of divalent cobalt ions which is 4.4–5.2 μ_B (17). Some deviations at high temperatures were apparent, which result from the contributions of the Van Vleck or temperature-independent paramagnetism. This contribution was found to be equal to 3.2×10^{-4} emu/mole.

2. $NiAs_2O_6$. Figure 6 shows the plot of the magnetic susceptibility data measured at 0.1 Tesla. The maximum in the susceptibility was 1.35×10^{-2} emu/mole and was observed at 30 K. Figure 6 shows the plot of the Curie–Weiss fit. The effective magnetic moment is 3.27(7) μ_B and θ is −66.2(8) K. Similar moment values were reported for Ni^{2+} ions as in $Ni(NH_3)_6Cl_2$, which has an effective moment of 3.2 μ_B (17). Some TIP contribution was observed and estimated at 4.0×10^{-4} emu/mole, which seems to be larger than those reported for other Ni^{2+} compounds.

Looking at Fig. 6, it can be seen that there are some deviations from the expected straight line of the Curie–Weiss law beginning below about 80 K. These deviations seem to indicate the presence of weak short-range correlations that are ferromagnetic in origin. This is a unique feature for $NiAs_2O_6$ that is not shared by the other two phases. Within the planes perpendicular to the c-axis, neighboring Ni^{2+} atoms are linked through bonds to oxygen atoms at angles of 90°. A ferromagnetic short-range order within the planes can be anticipated, as the Goodenough–Kanamori rules predict ferromagnetic interactions for this type of arrangement (19).

3. $MnAs_2O_6$. The susceptibility data of $MnAs_2O_6$ are plotted in Fig. 7 and the maximum value of 0.119 emu/mole is reached at about 13 K. The susceptibility data in the range between 20–280 K were fitted to a Curie–Weiss law, the results of which are plotted in Fig. 7. The effective magnetic moment obtained from this fit was 5.90(2)

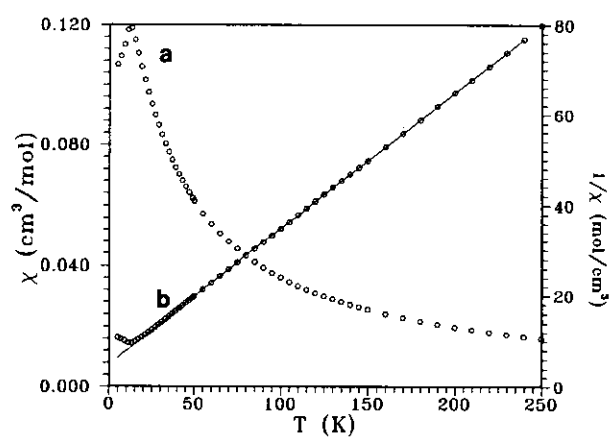

FIG. 7. (a) Magnetic susceptibility versus temperature for $MnAs_2O_6$; (b) the inverse of the magnetic susceptibility versus temperature. Circles represent the observed data and the solid line denotes the prediction of the Curie–Weiss fit.

TABLE 4
Magnetic Susceptibility Parameters for AAs_2O_6

Phase	$T(\chi_{max})$(K)	$\mu_{eff}(\mu_B)$	θ(K)	$TIP_{(cm^3/mole)}$	$R(\%)^a$
$NiAs_2O_6$	30	3.27(7)	−66.2(8)	4.0×10^{-4}	1.56
$CoAs_2O_6$	20	4.98(6)	−64.4(4)	3.2×10^{-4}	4.18
$MnAs_2O_6$	13	5.90(2)	−20.7(1)	0.0	1.23

^{a} $R(\%) = 100\ \{\Sigma(\chi_{obs} - \chi_{cal})^2/\Sigma\ \chi_{obs}^2\Sigma^{\frac{1}{2}}$.

μ_B and θ was −20.7(1). The Curie–Weiss law predictions fit the observed data rather well. This is because the ground state level of Mn^{2+} is ^6S, which is not split by the octahedral crystal field but gives rise to a $^6A_1$ term. This term is an orbital singlet, consequently it has no orbital angular momentum associated with it and spin-orbit coupling cannot raise the degeneracy of this term, which leads to a theoretical magnetic moment of 5.92 μ_B, i.e., a pure spin-only moment, which compares very well with the experimental moment for $MnAs_2O_6$.

Table 4 summarizes the experimental values of the susceptibility parameters for these arsenates.

This structure imposes restrictions on the distances and bond angles which connect the magnetic ions and hence dictate the potential superexchange pathways that can give rise to magnetic correlations. Figure 8 delineates the possible superexchange pathways in this structure in the (100) projection. Remarkably, the (100) projection resembles very closely the (001) projection of the trirutile structure except for the relative positions of the ligands. The nearest neighbor interaction J_1 involves the superexchange pathway A–O–A, with two unequal A–O bonds of 2.0 and 3.3 Å and an angle of 90°, and the next-nearest neighbor interaction J_4 involves the path A–O–O–A, where the angle A–O–O is 160° with an A–O bond distance of 2.0 Å and O–O bond distance of 2.4 Å. The absence of a dominating superexchange pathway could be the reason for the absence of any significant short-range order correlations in these oxides.

II. Long Range Order

Magnetic ordering in the triangular lattice has been a subject of many studies in the past (20–22). Antiferromagnetic ordering on a single triangular lattice is frustrated because at least one antiferromagnetic bond on each triangle must be broken. However, when triangular lattices are stacked along the third dimension and interplanar interactions are nonzero, long-range ordering can occur. This ordering is very dependent on the way magnetic ions are stacked with respect to each other. In these oxides, the magnetic ions form layers perpendicular to the c-axis. These layes are stacked in such a way that the sites of the magnetic ions are directly above and below each other with no offset in the ⟨100⟩ or ⟨010⟩ directions, which results in what is known as ...AAA... stacking. Reimers and Dahn (9) studied the effect of this and other stacking patterns on long-range order in the triangular spin systems using the mean field theory formalism. They studied the effect of the relative strength of the in-plane and interplane interactions in stabilizing a particular ordered state. For systems with small interplanar spacings, as in these arsenates, the interplanar interactions might be more important than the in-plane interactions. In such cases, the mean field calculations predicted that the phase diagram is divided into regions characterized by the wavevectors $(\frac{1}{3}, \frac{1}{3}, 0)$ and $(0, 0, \frac{1}{2})$.

To further investigate the magnetically ordered state, low-temperature neutron diffraction data were collected for these compounds. In all cases additional superlattice reflections were observed to disappear above their respective T_c's, suggesting that these additional superlattice reflections are magnetic in nature.

1. Magnetic structure of $NiAs_2O_6$. Neutron diffraction data were collected at 10, 20, 25, 28, and 30 K in the 2θ range 6–35°. The results can be summarized by considering the data at five temperatures as shown in Fig. 9 in

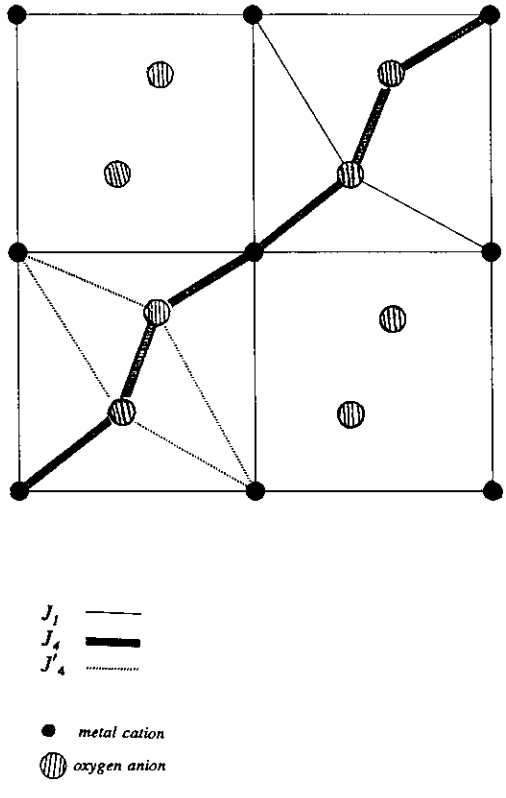

FIG. 8. The possible superexchange pathways in the AAs_2O_6 compounds.

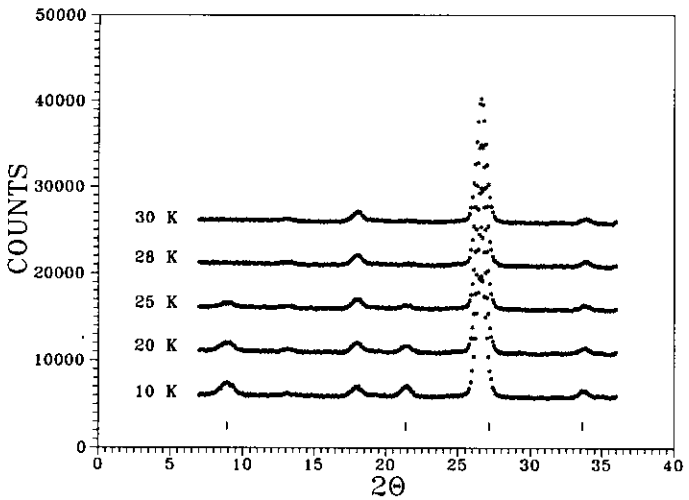

FIG. 9. Low-temperature neutron scattering data for $NiAs_2O_6$ collected at various temperatures. The superlattice reflections are indicated by vertical bars.

which two superlattice reflections at 2θ angles of 8.88 and 21.48° can observed to gradually decrease in intensity until they disappear at about 30 K, indicating that they are magnetic in origin. These magnetic peaks can be indexed on a magnetic cell of a_c and $2c_c$ (a_c and c_c are the chemical cell constants), i.e., a magnetic propagation vector $k = (00\frac{1}{2})$, so that these peaks can be indexed as (001) and (003) on the magnetic cell.

The refinement was carried out in the space group $P\text{-}31m$. Figure 10 shows a good fit of this model to the observed data with $R_{wp} = 6.08$, $R_p = 4.50$, and $R_{exp} = 4.10$. The atomic positions and the cell parameters were fixed during the refinement. The scale, background, full width at half-maximum parameters (U, V, W), overall temperature factor, asymmetry parameter, preferred orientation, magnetic moment, and angle ϕ were refined. The magnetic moment of Ni^{2+} obtained was 2.11(3) μ_B, which compares well with the magnetic moments reported in the literature such as the magnetic moment in Ni^{2+} in $KNiF_3$ with $\mu = 2.2$ μ_B (23) and in K_2NiF_4 with $\mu = 1.9$ μ_B (24). The angle ϕ was refined to 61(6)°; the large standard deviation in the angle ϕ would make it not very reliable. Fixing the angle at 90° gives a worse fit with $R_{wp} = 8.2$.

Based on the above results, the spin arrangements in this compound can be described as consisting of an alternating sequence of ferromagnetic (001) layers coupled antiferromagnetically.

In principle, this compound can undergo a metamagnetic transition, i.e., a field-induced transition from the antiferromagnetic state directly to the saturated paramagnetic phase. Such a possibility was further investigated by measurng the magnetic susceptibility as a function of temperature at various magnetic field strengths. These results are summarized in Figure 11, in which the antiferromagnetic transition persists even at 5 Tesla, which rules out the presence of the metamagnetic transition in this field range.

2. Magnetic structure of $CoAs_2O_6$. Similar measurements at low temperatures as those performed on the $NiAs_2O_6$ were done on this sample. Low-temperature neutron diffraction data were collected at 9, 12, 17, 18, 19, and 19.5 K. These superlattice reflections were observed at the 2θ angles of 8.75, 21.27, and 35.10°, which then disappeared above about 20 K. This temperature corresponds to the ordering temperature as indicated in

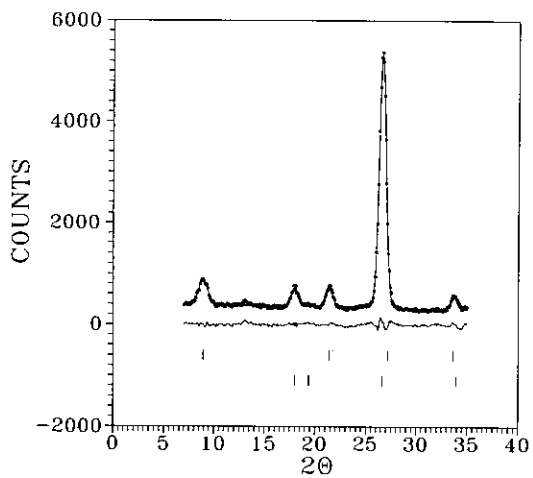

FIG. 10. The Rietveld refinement fit of the magnetic scattering data for $NiAs_2O_6$. The upper set of bars indicates the magnetic Bragg peaks and the lower set corresponds to the nuclear Bragg peaks.

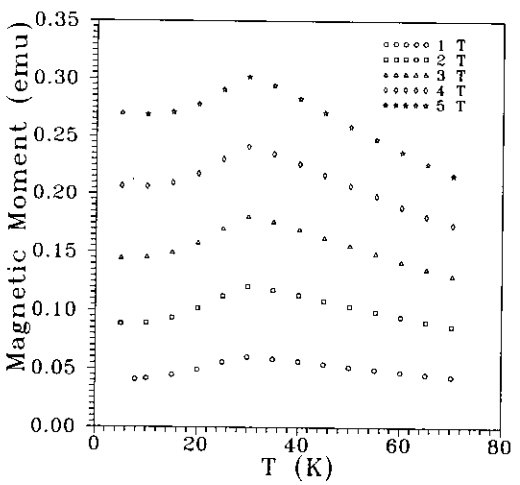

FIG. 11. Variation of the magnetic moment as a function of field for $NiAs_2O_6$. The magnetic moment is shown versus temperature at various magnetic fields.

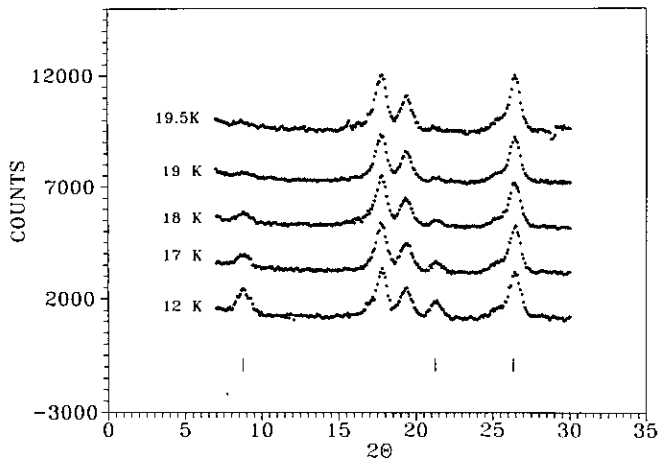

FIG. 12. Low-temperature neutron scattering data for $CoAs_2O_6$ at various temperatures. The superlattice reflections are indicated by the vertical bars.

the magnetic susceptibility data, suggesting that these superlattice reflections are magnetic in origin. The neutron diffraction results are summarized in Fig. 12, in which the intensity of the superlattice reflections decreases as the temperature is increased and finally vanishes at about 19.5 K. As in the case of $NiAs_2O_6$, these superlattice reflections can be represented by a propagation vector $k = (00\frac{1}{2})$ and were indexed as (001), (003), and (111), respectively.

Likewise, the refinement was carried out in the space group $P\text{-}31m$. The atomic positions and the cell parameters were fixed during the refinement. The magnetic moment of each magnetic site and the angle between the spin direction and the unique axis of the lattice, ϕ, were refined. A reasonable fit was obtained with the R factors $R_{wp} = 7.86$, $R_p = 5.85$, and $R_{exp} = 4.13$. The profile pattern of the fit is plotted in Fig. 13. The refined magnetic moment of Co^{2+} ion was 2.66(30) μ_B, which is somewhat smaller than other reported magnetic moments for Co^{2+}, for example, $RbCoF_3$ with μ of 3.0 μ_B (25) and CoO with μ of 3.5 μ_B (26). The angle between the spin direction and the c-axis, ϕ, is 66(16)°. The standard deviation of ϕ in this case is even larger than that for $NiAs_2O_6$, but it resulted in an improvement of the fit which is evident from the fact that a refinement carried out with the parameter ϕ fixed at 90° gives an R_{wp} of 9.30.

Since the intensity of the magnetic scattering at zero field is proportional to the square of the spontaneous magnetization, the temperature dependence of the intensity of the magnetic peaks yields the behavior of the magnetization and thus the critical exponent β. It was possible to estimate the critical exponent β and the critical temperature T_c by using the intensity of the magnetic reflection (001) obtained from the neutron diffraction data between 9 and 19.5 K. The values for T_c and β were determined from a least-squares refinement of the relationship

$$M \alpha \left(\frac{T - T_c}{T_c}\right)^{\beta},$$

where M is the spontaneous magnetization and β is the magnetization critical exponent. A log–log plot, Fig. 14, of the spontaneous magnetization versus reduced temperature, t, gives $T_c = 19.1(2)$ and $\beta = 0.27(5)$. The value of β is closest to that of the 3-D Ising system, which predicts a β value of 0.3125 (27).

As in $NiAs_2O_6$, the phase transition in the susceptibility persisted when measured in magnetic fields up to 5 T indicating that no metamagnetic transition is present in this material as well.

The magnetic ordering in both $NiAs_2O_6$ and $CoAs_2O_6$ is in accordance with those predicted by Reimers' calculations for systems with large interplanar interactions. Similar behavior was reported for $FeCl_2$ and $FeBr_2$, which also crystallize in the space group $P\text{-}3m1$ and where the Fe^{2+} sublattice forms a hexagonal lattice with an ...AA... stacking (28). Davidson also reported an identical magnetically ordered state for $1T\text{-}Li_2NiO_2$ (29).

3. Magnetic scattering of $MnAs_2O_6$. Low-temperature neutron diffraction data for this material were collected on the Dualspec diffractometer with 1.50-Å neutrons. A difference plot of the 5 K and the room-temperature data is shown in Fig. 15 in which a number of superlattice reflections were observed that disappeared at about 12 K.

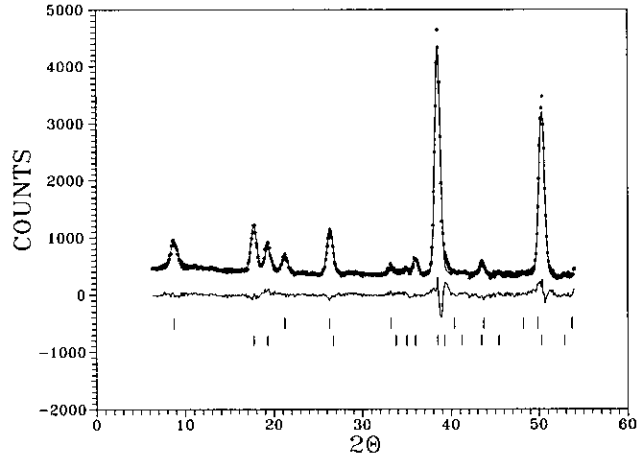

FIG. 13. The Rietveld refinement fit of the magnetic scattering data for $CoAs_2O_6$. The upper set of bars indicates the magnetic Bragg peaks and the lower set corresponds to the nuclear Bragg peaks.

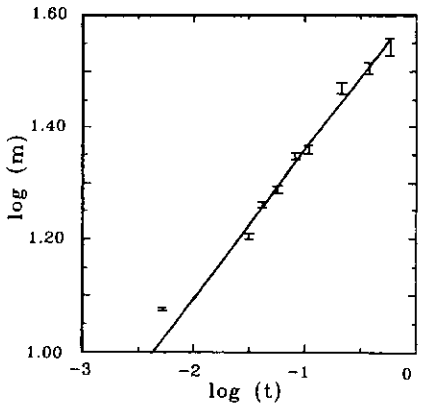

FIG. 14. Log–log plot of the magnetic moment versus the reduced temperature for $CoAs_2O_6$.

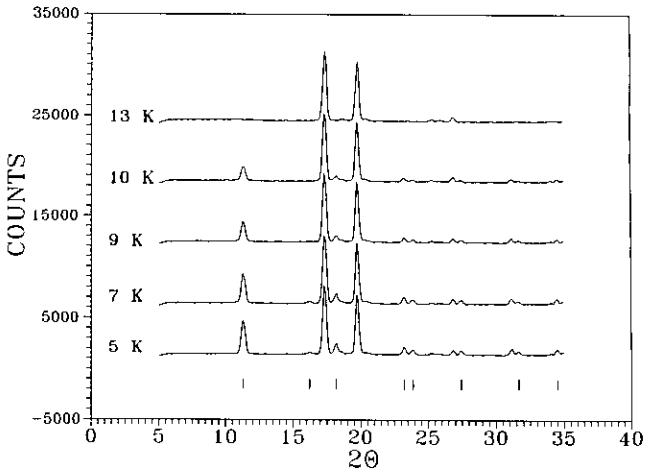

FIG. 16. The variation of the intensity of the superlattice reflections as a function of temperature for $MnAs_2O_6$.

The vanishing of these superlattice reflections is clearly shown in Fig. 16 in which the intensity of the magnetic peaks was traced as the temperature was increased. It was obvious that these superlattice reflections cannot be indexed by the simple propagation vector $k = (00\frac{1}{2})$, as in $CoAs_2O_6$ and $NiAs_2O_6$. An extensive search for a commensurate magnetic unit cell was carried out in which the combinations $(2a, 2a, 2c)$, $(2a, a, 2c)$, $(3a, 3a, 2c)$, $(3a, 3a, c)$, $(\sqrt{3}a, \sqrt{3}a, 2c)$, and $(2\sqrt{3}a, 2\sqrt{3}a, 2c)$ were tried in order to index the superlattice reflections but without success. We were able to fit all of the superlattice reflections with an incommensurate propagation vector $k = (0.055, 0.389, 0.136)$ in r.l.u. The quality of the solution was judged by the use of the mean square deviation in the d-spacing.

$$\Delta d_{\mathrm{RMS}} = [\Sigma\ (d_{\mathrm{cal}} - d_{\mathrm{obs}})^2]^{1/2},$$

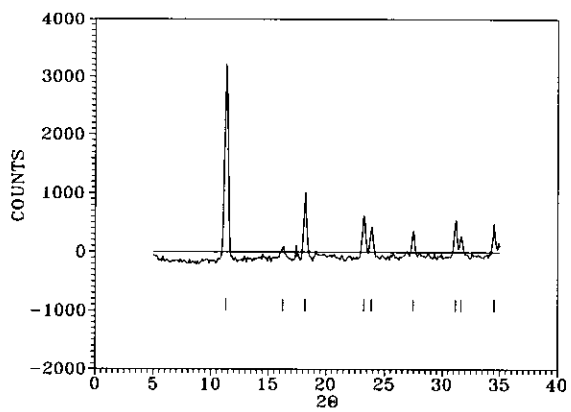

FIG. 15. The difference plot of the 5 K neutron scattering data set and 15 K data set for $MnAs_2O_6$. The vertical bars underneath represent the positions of the superlattice reflections.

which was found to be 0.016 Å for all the indexed peaks, indicating a reasonable fit. Remarkably, in contrast with those of the isostructural $NiAs_2O_6$ and $CoAs_2O_6$, the magnetic ordered state in $MnAs_2O_6$ is very complicated. Incommensurate magnetic ordering is rarely observed for systems with ...AAA... stacking and was obtained in the mean field calculations only if further in-plane interactions were included. Similar behavior was observed for the isostructural members $CsMnBr_3$ and $RbMnBr_3$, in which the system $CsMnBr_3$ (30) was found to order with the 120° spin structure, $k = (\frac{1}{3}, \frac{1}{3}, 0)$, while the material $RbMnBr_3$ (31) adopts an incommensurate magnetic structure with the wavevector $k = (0.357, 0.357, 0)$. Attempts to find solutions in the XY plane for $MnAs_2O_6$ were not successful where the z-component of the propagation vector was fixed at 0, $\frac{1}{4}$, and $\frac{1}{2}$. This is likely to be a result of the fact that both the in-plane and the interplanar interactions are important in stabilizing the incommensurate ordered state in this system. This is interesting because such a behavior is more likely to be expected in systems with ...ABAB... or ...ABCAB... stackings in which their phase diagrams are dominated by regions of incommensurate wavevectors (9).

ACKNOWLEDGMENTS

We thank Dr. J. N. Reimers for his assistance with the indexing of the $MnAs_2O_6$ diffraction pattern and for many useful discussions about incommensurate structures. We thank Dr. Stager for the use of the SQUID magnetometer and F. Gibbs for collecting the thermogravimetric data. This work was supported by the Natural Science and Engineering Research Council of Canada. A. M. Nakua acknowledges the financial support of the Secretariat for Scientific Research of Libya.

REFERENCES

1. S. M. Eicher, J. E. Greedan, and K. Lushington, *J. Solid State Chem.* **62,** 220 (1986); S. M. Eicher, Ph.D. Dissertation, McMaster University, 1984.
2. J. N. Reimers, J. E. Greedan, C. Stager, and R. Kremer, *J. Solid State Chem.* **83,** 20 (1989).
3. J. E. Greedan, *Landolt-Bornstein New Ser. III/27g,* 1992.
4. A. Magneli, *Arkiv. Kemi Mineral. Geol.*, **15B,** 1 (1941).
5. J. Taylor and R. Hyde, *Can. J. Chem.* **36,** 597 (1958).
6. A. Kasper, *Mh. Chem* **98,** 2107 (1967).
7. R. Hill, *J. Solid State Chem.* **71,** 12 (1987).
8. M. Wildner, *Z. Kristallogr.* **202,** 51 (1992).
9. J. N. Reimer and J. Dahn, *J. Phys. Condens. Matter* **4,** 8105 (1992).
10. A. Wells, "Structural Inorganic Chemistry," 5th ed., p. 905. Oxford Science, London, 1984.
11. J. N. Reimers, J. E. Greedan, and M. Sato, *J. Solid State Chem.* **72,** 390 (1988).
12. R. Sakthivel and R. Young, "User's Guide to Programs DBWS-9006 and DBWS-9006PC," 1991; D. B. Wiles and R. A. Young, *J. Appl. Crystallogr.* **14,** 149 (1981).
13. F. Izumi, "Rietan–Rietveld Analysis Systems, National Institute for Research in Inorganic Materials, Ibaraki"; *Nippon Kessho Gakkai shi* **27,** 23 (1995).
14. G. Shirane, *Acta Crystallogr.* **12,** 282 (1959).
15. R. Watson and A. Freeman, *Acta Crystallogr.* **14,** 27 (1961).
16. L. Mulay, "Magnetic Susceptibility." Interscience, New York, 1966.
17. A. Earnshaw, "Introduction to Magnetism." Academic Press, New York, 1968.
18. J. Goodenough, *Phys. Rev.* **100,** 564 (1955); J. Goodenough, *J. Phys. Chem. Solids* **6,** 287 (1958); J. Kanamori, *J. Phys. Chem. Solids* **10,** 87 (1959).
19. Deleted in proof.
20. D. Blankschtein, M. Ma, A. Berker, G. Grest, and C. Soukoulis, *Phys. Rev. B* 5250 (1984).
21. F. Matsubara and I. Sakari, *J. Phys. Soc. Jpn.* **56,** 2666 (1987); **56,** 4087 (1987).
22. J.-J. Kim, Y. Yamada, and O. Nagai, *Phys. Rev.* **41,** 4760 (1990).
23. V. Scatturin, L. Corliss, N. Elliott, and J. Hastings, *Acta Crystallogr.* **14,** 19 (1961).
24. R. Brigeneau, H. Guggeneim, and G. Shirane, *Phys. Rev. B* **1** 2211 (1970).
25. Y. Allain, *J. Phys. C* **23,** 611 (1971).
26. D. Khan and R. Erickson, *Phys. Rev. B* **1** 2243 (1970).
27. F. Fava, M. Danot, N. Dinh, A. Daoudi, and G. LeFlem, *Solid State Commun.* **22,** 733 (1977).
28. A. Wiedenmann, L. P. Regnault, P. Burlet, and J. Rossat-Mignod, *J. Magn. Magn. Mater.* **74,** 7 (1988).
29. I. J. Davidson, J. E. Greedan, U. Von Sacken, C. A. Michal, and W. R. McKinnon, *J. Solid State Chem.* **105,** 410 (1993).
30. M. Eibschutz, R. Sherwood, F. Hsu, and D. Cox, *in* "Conference on Magnetism and Magnetic Materials 1972" (C. Graham, Jr., and J. Rhyne, Eds.), Part 1, p. 684, AIP Conf. Proc., Vol. 10. Am. Inst. of Phys., New York, 1973.
31. G. Glinka, V. Minkiewicz, D. Cox, and C. Kjatak, *in* "Conference on Magnetism and Magnetic Materials 1972" (C. Graham, Jr., and J. Rhyne, Eds.), Part 1, p. 659, AIP Conf. Proc., Vol. 10. Am. Inst. of Phys., New York, 1973.